

## Bandwidth extension of narrowband-signal intensity calculation using additive, low-level broadband noise

Mylan R. Cook, Kelli F. Succo, Kent L. Gee, Scott D. Sommerfeldt, and Tracianne B. Neilsen

Citation: *The Journal of the Acoustical Society of America* **145**, 3146 (2019); doi: 10.1121/1.5108661

View online: <https://doi.org/10.1121/1.5108661>

View Table of Contents: <https://asa.scitation.org/toc/jas/145/5>

Published by the [Acoustical Society of America](#)

---

### ARTICLES YOU MAY BE INTERESTED IN

[Sound field reconstruction using inverse boundary element method and sparse regularization](#)

*The Journal of the Acoustical Society of America* **145**, 3154 (2019); <https://doi.org/10.1121/1.5109393>

[Pharyngeal flow simulations during sibilant sound in a patient-specific model with velopharyngeal insufficiency](#)

*The Journal of the Acoustical Society of America* **145**, 3137 (2019); <https://doi.org/10.1121/1.5108889>

[Cross-correlation of shipping noise: Refraction and receiver-motion effects](#)

*The Journal of the Acoustical Society of America* **145**, 3003 (2019); <https://doi.org/10.1121/1.5108602>

[Superdirective beamforming applied to SWellEx96 horizontal arrays data for source localization](#)

*The Journal of the Acoustical Society of America* **145**, EL179 (2019); <https://doi.org/10.1121/1.5092580>

[A three-dimensional underwater sound propagation model for offshore wind farm noise prediction](#)

*The Journal of the Acoustical Society of America* **145**, EL335 (2019); <https://doi.org/10.1121/1.5099560>

[Envelope regularity discrimination](#)

*The Journal of the Acoustical Society of America* **145**, 2861 (2019); <https://doi.org/10.1121/1.5100620>

---



CAPTURE WHAT'S POSSIBLE  
WITH OUR NEW PUBLISHING ACADEMY RESOURCES

Learn more 



# Bandwidth extension of narrowband-signal intensity calculation using additive, low-level broadband noise

Mylan R. Cook,<sup>a)</sup> Kelli F. Succo, Kent L. Gee, Scott D. Sommerfeldt, and Tracianne B. Neilsen

*Department of Physics and Astronomy, Brigham Young University, N283 ESC Provo, Utah 84602, USA*

(Received 4 January 2019; revised 19 April 2019; accepted 25 April 2019; published online 30 May 2019)

Calculation of acoustic intensity using the phase and amplitude gradient estimator (PAGE) method has been shown to increase the effective upper frequency limit beyond the traditional p-p method when the source of interest is broadband in frequency [Torrie, Whiting, Gee, Neilsen, and Sommerfeldt, *Proc. Mtgs. Acoust.* **23**, 030005 (2015)]. PAGE processing calculates intensity for narrowband sources without bias error up to the spatial Nyquist frequency [Succo, Sommerfeldt, Gee, and Neilsen, *Proc. Mtgs. Acoust.* **30**, 030015 (2018)]. The present work demonstrates that for narrowband sources with frequency content above the spatial Nyquist frequency, additive low-level broadband noise can improve intensity calculations. To be effective, the angular separation between the source and additive noise source should be less than 30°, while using phase unwrapping with a smaller angular separation will increase the usable bandwidth. The upper frequency limit for the bandwidth extension depends on angular separation, sound speed, and probe microphone spacing. Assuming the signal-to-additive-noise ratio (SNR<sub>a</sub>) is larger than 10 dB, the maximum level and angular bias errors incurred by the additive broadband noise beneath the frequency limit—or up until probe scattering effects must be taken into account—are less than 0.5 dB and 2.5°, respectively. Smaller angular separation yields smaller bias errors. © 2019 Acoustical Society of America. <https://doi.org/10.1121/1.5108661>

[KGS]

Pages: 3146–3153

## I. INTRODUCTION

Active acoustic intensity, simply referred to as intensity hereafter, is an energy-based acoustic measure obtained by the product of acoustic pressure and particle velocity. As a vector quantity, it gives the magnitude and direction of the propagating acoustic energy. Intensity is often used for source characterization, since the direction of propagation can identify which regions of a source are radiating more dominantly.<sup>1</sup> Many additional applications of intensity have been explored.<sup>2–4</sup>

Acoustic intensity can be computed in several ways; one of the most prevalent methods is referred to as the p-p method, in which a probe with multiple microphones is used to estimate the gradient of pressure by using the change in the real and imaginary pressure components divided by the microphone spacing.<sup>5–7</sup> The p-p method is hereafter referred to as the traditional method. One significant limitation of the traditional method is that the microphone spacing must be small relative to the acoustic wavelength. The particle velocity is underestimated when the microphone spacing begins to be sufficiently large relative to a wavelength, which leads to errors at high frequencies. At much lower frequencies, inherent or residual microphone phase mismatch can cause significant errors. Between these two frequency limitations, there is only a fairly limited bandwidth over which the traditional method can be adequately used. These and other errors have been discussed at length,<sup>8–14</sup> and many have tried to overcome the errors using varying experimental sensor placement or processing.<sup>15–18</sup>

To overcome some of the problems of the traditional method, especially for high-amplitude jet and rocket noise, the phase and amplitude gradient estimator (PAGE) method was developed.<sup>19–21</sup> Instead of using formulations which split the complex pressure into real and imaginary parts, as is done in the traditional method, the formulations for the PAGE method represent the complex pressure with a magnitude and phase, based on expressions from Mann *et al.*<sup>22</sup> and Mann and Tichy.<sup>1,23</sup> The expression for intensity with the PAGE method is

$$\mathbf{I} = \frac{1}{\rho_0 \omega} P^2 \nabla \phi, \quad (1)$$

where  $P$  represents the pressure magnitude and  $\nabla \phi$  represents the pressure phase gradient, where  $\rho_0$  is the air density and  $\omega$  is the angular frequency. These expressions are advantageous—particularly in propagating fields—because the pressure magnitude and phase manifest less spatial variation than the real and imaginary components of pressure, which allows for a more accurate estimation of the particle velocity across a wider range of frequencies.

Using the PAGE method allows for calculation of intensity at much higher frequencies than does the traditional method. The bias errors for both methods have been investigated,<sup>20,21</sup> and in general the bias errors for the PAGE method are less than or equal to those of the traditional method. The effects of contaminating noise on both methods have likewise been investigated.<sup>30</sup>

The PAGE method generally relies upon phase information in broadband signals to obtain valid intensity results at

<sup>a)</sup>Electronic mail: mylan.cook@gmail.com

frequencies above the probe spatial Nyquist frequency, denoted  $f_N$ , by using phase unwrapping. With narrowband signals, phase information can be sparse enough that the phase gradient may not be calculated reliably above  $f_N$ . For distinct tones, the sparsity of phase information in frequency space can make calculation of intensity at these higher frequencies especially erroneous. Fortunately, there is a simple solution. When more phase information is lacking, additive low-level broadband noise with similar directionality can often provide phase information so that the PAGE method can be used effectively with narrowband signals—whether tonal or band-limited—above  $f_N$ .

This paper discusses the theoretical and experimental effects of additive broadband noise on obtaining intensity estimates for narrowband signals, specifically tonal frequencies. In Sec. II, the theory for additive broadband noise is developed. The analytical bias errors are presented in Sec. III. In Sec. IV experimental results are presented and compared to the analytical results, with conclusions following in Sec. V.

## II. METHODOLOGY

In this section, the mathematical theory for how additive broadband noise can improve intensity calculation for narrowband signals is developed. Necessary parameters are discussed, followed by the mathematical derivations and bias errors. Practical simplifications are then made, and a guide to when additive broadband noise is helpful is provided.

### A. Preliminary parameters

#### 1. Spatial Nyquist frequency

With the traditional method, the effective upper frequency limit for reliable intensity calculation is the spatial Nyquist frequency,  $f_N$ : the frequency at which the microphone spacing,  $a$ , is equal to half of an acoustic wavelength,  $f_N = c/2a$ , where  $c$  is the sound speed. Including possible probe rotations— $\theta_S$ , discussed in Sec. II B—this becomes  $f_N = c/2a \cos \theta_S$ . This spatial sampling requirement means that microphones in an intensity probe must be placed closer together to calculate intensity for higher frequencies, which can not only increase the effects of scattering, but also increase phase mismatch errors at lower frequencies. Probe configuration and orientation can change the effective microphone spacing and yields an effective spatial Nyquist frequency,  $f_{N,\text{eff}}$ . As  $f_{N,\text{eff}}$  is approached—even at frequencies below  $(1/2)f_{N,\text{eff}}$ —the particle velocity is underestimated by the traditional method, so calculated intensities are only reliable well below  $f_{N,\text{eff}}$ . In general, angular estimates are valid up to frequencies near  $f_{N,\text{eff}}$ , while magnitude estimates are only valid up to around one-half of  $f_{N,\text{eff}}$ .<sup>24</sup> However, the PAGE method yields accurate magnitude and phase estimates up to  $f_{N,\text{eff}}$  and also at higher frequencies if the phase gradient can be accurately calculated. Accurate calculation requires the use of phase unwrapping.

#### 2. Phase unwrapping

To calculate the phase gradient, the phases of the transfer functions between microphone pairs are used. Because

the phase differences obtained from transfer functions are restricted to a  $2\pi$  radian interval, a linear phase difference in frequency space wraps or jumps between  $\pi$  radians and  $-\pi$  radians at odd integer multiples of  $f_{N,\text{eff}}$ , as illustrated by the solid line in Fig. 1. The phase is unwrapped by adding multiples of  $2\pi$  radians to create a continuous phase relationship (dashed line in Fig. 1). In this manner, the correct overall phase gradient can be obtained.<sup>25–29</sup>

Phase unwrapping works well for broadband signals with sufficient coherence between microphones, most especially for signals with a linear phase relationship.<sup>31</sup> For narrowband signals, or signals composed of discrete frequencies, however, the sparsity of frequency-dependent phase information can cause problems with phase unwrapping. Incorrectly unwrapped phase values lead to inaccurate phase gradient estimates and, therefore, incorrect intensity vectors for frequencies above  $f_{N,\text{eff}}$ . As seen in Fig. 1, the phase gradient obtained for peak frequencies from inaccurately unwrapped phase values can be extremely flawed and can even trend in the opposite direction. Wrapped phase values at frequencies where there is a signal, hereafter referred to as peak frequencies, are measured for the source, but can be sparse. In contrast, for frequencies without a signal—called noise frequencies—the phase values come from the ambient noise rather than from the source. These phase values have no relation to the phase that would be caused by the source at that frequency, and so are not valid for source properties. Phase unwrapping for narrowband signals is therefore prone to error without additional phase information, which is where additive low-level broadband noise can be helpful.

### 3. Signal-to-noise ratios

The effects of and bias errors caused by contaminating noise in the sound field have been previously investigated.<sup>30</sup> When the signal-to-noise ratio (SNR) is sufficiently large,

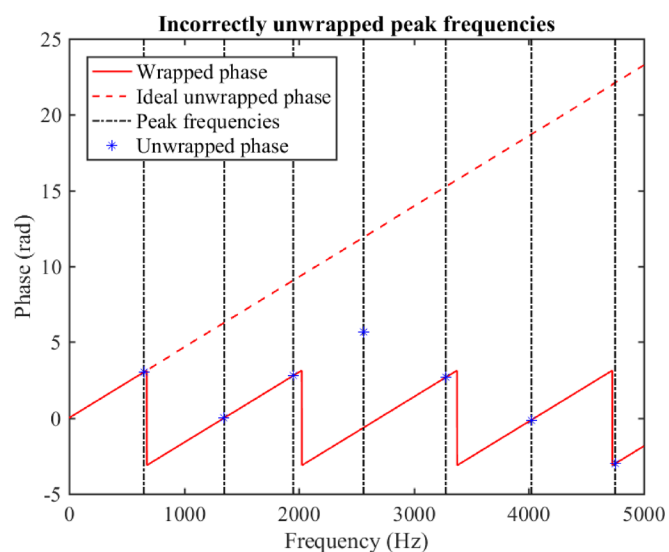


FIG. 1. (Color online) An example of ideal wrapped and unwrapped phase values (red) for a broadband signal coming from the same angular direction as a narrowband signal. The sparsity of phase information—none between peak frequencies (black)—for the narrowband signal leads to unreliable unwrapped phase values (blue), and can therefore lead to flawed phase gradient estimates for narrowband signals.

the contaminating noise does not significantly affect the calculation of intensity. For narrowband sources where frequencies of interest are above  $f_N$ , additive broadband noise can actually be helpful. While ambient noise is more or less isotropic, which leads to random phase directions, additive noise can be directional. Additive broadband noise can thus provide coherent phase information across the probe at noise frequencies, which can improve unwrapping and, therefore, lead to better intensity calculations. The additive noise must necessarily be higher in level than the ambient noise, which is quantified by comparing two signal-to-noise ratios: The signal-to-additive-noise ratio is denoted by  $\text{SNR}_a$ , while the signal-to-ambient-noise ratio is simply the usual SNR. When  $\text{SNR}_a < \text{SNR}$ , the additive noise can provide coherent phase information, which can allow for meaningful phase unwrapping, which results in more accurate phase gradient estimates at peak frequencies. Ideally, the  $\text{SNR}_a$  should be significantly smaller than the SNR, because when the two are close (within a few dB) the phase information of the ambient noise may influence the phase of the additive noise.

## B. Mathematical foundation

### 1. Derivations

The benefit of additive noise can be illustrated using the five-microphone orthogonal probe pictured in Fig. 2. This probe is chosen because symmetry can be employed and calculations are simplified by using pairs of orthogonal microphones.<sup>24</sup> The intensity for this probe using the PAGE method calculation is

$$I_{\text{calc}} = \frac{-G_{11} \arg\{H_{23}\}}{4k\rho_0 c} \hat{x} + \frac{-G_{11} \arg\{H_{45}\}}{4k\rho_0 c} \hat{y}, \quad (2)$$

where  $G_{11}$  is the auto-spectrum of the central microphone,  $H_{\mu\nu}$  is the transfer function between microphones  $\mu$  and  $\nu$ ,  $c$  is the sound speed,  $\rho_0$  is the air density, and  $k$  is the wavenumber. Microphones 2, 1, and 3 lie along the  $\hat{x}$  axis, while microphones 5, 1, and 4 lie along the  $\hat{y}$  axis, where microphone 1 is at the probe center and defines the origin, as explained in the caption for Fig. 2. For a plane wave source of pressure

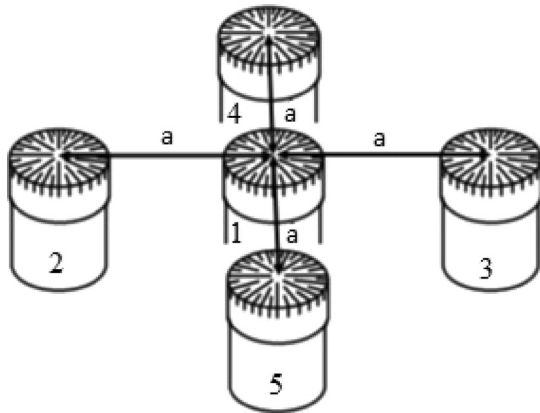


FIG. 2. A five-microphone orthogonal probe. The microphones are numbered 1 to 5, and have positions  $(x,y) = (0,0)$ ,  $(-a,0)$ ,  $(a,0)$ ,  $(0,a)$ , and  $(0,-a)$ , respectively.

amplitude  $A_s$  coming from an angle  $\theta_s$ , and additive plane wave noise—which is self-correlated, though uncorrelated with the source<sup>30</sup>—of amplitude  $A_n$  coming from an angle  $\theta_n$ ,

$$G_{11} = A_s^2 + A_n^2, \quad (3)$$

$$\arg\{H_{23}\} = \arg\{A_s^2 e^{-2jka \cos \theta_s} + A_n^2 e^{-2jka \cos \theta_n}\}, \quad (4)$$

$$\arg\{H_{45}\} = \arg\{A_s^2 e^{-2jka \sin \theta_s} + A_n^2 e^{-2jka \sin \theta_n}\}. \quad (5)$$

For the peak frequencies of a narrowband signal with low-level additive noise,  $A_s^2 \gg A_n^2$ , so the additive noise causes a negligibly small change in transfer function arguments. At noise frequencies there is no signal, i.e.,  $A_s \approx 0$ , and the transfer function phase values obtained from the additive noise are used for unwrapping. The signal-only values at peak frequencies are  $G_{11} = A_s^2$ ,  $\arg\{H_{23}\} = -2ka \cos \theta_s$ , and  $\arg\{H_{45}\} = -2ka \sin \theta_s$ . As long as the angular separation  $|\theta_s - \theta_n|$  is not too large, these values can be obtained, as is further outlined below. When there is any angular separation, some error is unavoidably introduced.

When angular separation becomes too large, phase unwrapping can fail, which causes inaccurate intensity calculation. The frequency resolution used in processing  $\Delta f$  also has an impact on the unwrapping—too few points between peak frequencies results in poor unwrapping. The phase can be unwrapped correctly if the phase difference of the transfer functions at the peak frequency,  $f_p$ , and the adjacent noise frequency,  $f_n = f_p \pm \Delta f$ , is less than  $\pi$  radians, i.e.,

$$|\arg\{H_{23}(f_p)\} - \arg\{H_{23}(f_p \pm \Delta f)\}| \leq \pi, \quad (6)$$

$$|\arg\{H_{45}(f_p)\} - \arg\{H_{45}(f_p \pm \Delta f)\}| \leq \pi. \quad (7)$$

Note that for band-limited signals rather than for discrete tones,  $f_p \pm \Delta f$  is not necessarily a noise frequency. Equations (6) and (7) do not need to be checked for validity in this case, only when  $f_p \pm \Delta f$  is a noise frequency; the latter case is where the phase values exhibit the greatest change. The frequency when these inequalities are no longer satisfied defines an upper frequency limit,  $f_{\text{lim}}$ , above which the bias errors sharply increase since unwrapping fails. By assuming  $A_s^2(f_p) \gg A_n^2(f_p)$  and  $A_s^2(f_n) \approx 0$  [a relatively large signal-to-additive-noise ratio ( $\text{SNR}_a$ ) and a negligible signal amplitude at noise frequencies] and solving for the maximum value of  $f$  where Eqs. (6) and (7) hold, the maximum frequency value is found to be

$$f_{\text{lim}} = \min \left\{ \frac{c - 4a\Delta f |\cos \theta_n|}{4a |\cos \theta_n - \cos \theta_s|}, \frac{c - 4a\Delta f |\sin \theta_n|}{4a |\sin \theta_n - \sin \theta_s|} \right\}. \quad (8)$$

This value gives the upper frequency limit for when additive low-level broadband noise will help improve intensity calculation above  $f_N$ .

### 2. Bias errors

When only frequencies below  $f_{\text{lim}}$  are considered, the bias errors for the calculated intensity due to additive noise are small. An example of the bias error is shown by considering a

plane-wave signal consisting of a series of discrete peak frequencies. The analytical intensity for the plane wave signal of pressure amplitude  $A_s$  travelling in the  $\theta_s$  direction is

$$I(\omega) = \frac{A_s^2(\omega)}{2\rho_0 c} \hat{\theta}_s. \quad (9)$$

The magnitude and direction bias errors are calculated, respectively, as

$$\begin{aligned} L_{\epsilon, I} &= 10 \log_{10} \left( \sqrt{\left| \frac{-G_{11} \arg\{H_{23}\}}{2kaA_s^2} \right|^2 + \left| \frac{-G_{11} \arg\{H_{45}\}}{2kaA_s^2} \right|^2} \right) \\ &= 10 \log_{10} \left( 1 + \frac{A_n^2}{A_s^2} \left( 1 + \frac{\sin(2ka(\cos \theta_n - \cos \theta_s))}{2ka} \cos \theta_s + \frac{\sin(2ka(\sin \theta_n - \sin \theta_s))}{2ka} \sin \theta_s \right) + O\left(\frac{A_n^4}{A_s^4}\right) \right) \\ &= 10^{1-\text{SNR}_a/10} \left( 1 + \frac{\sin(2ka(\cos \theta_n - \cos \theta_s))}{2ka} \cos \theta_s + \frac{\sin(2ka(\sin \theta_n - \sin \theta_s))}{2ka} \sin \theta_s \right) + O(10^{-2*\text{SNR}_a/10}), \end{aligned} \quad (12)$$

while the angular bias in radians is given by

$$\begin{aligned} \theta_{\epsilon, I} &= \tan^{-1} \frac{-\arg\{H_{45}\}}{-\arg\{H_{23}\}} - \theta_s = \tan^{-1} \frac{-\arg\{A_s^2 e^{-2jka \sin \theta_s} + A_n^2 e^{-2jka \sin \theta_n}\}}{-\arg\{A_s^2 e^{-2jka \cos \theta_s} + A_n^2 e^{-2jka \cos \theta_n}\}} - \theta_s \\ &= \frac{A_n^2}{A_s^2} \left( \frac{\sin(2ka(\sin \theta_n - \sin \theta_s))}{2ka} \cos \theta_s - \frac{\sin(2ka(\cos \theta_n - \cos \theta_s))}{2ka} \sin \theta_s \right) + O\left(\frac{A_n^4}{A_s^4}\right) \\ &= 10^{-\text{SNR}_a/10} \left( \frac{\sin(2ka(\sin \theta_n - \sin \theta_s))}{2ka} \cos \theta_s - \frac{\sin(2ka(\cos \theta_n - \cos \theta_s))}{2ka} \sin \theta_s \right) + O(10^{-2*\text{SNR}_a/10}). \end{aligned} \quad (13)$$

The maximum errors across  $\theta_s$  and  $\theta_n$  for frequencies below  $f_{\text{lim}}$  can be obtained from (the exact solutions of) Eqs. (12) and (13) to give the maximum error as a function of only  $\text{SNR}_a$ :

$$|L_{\epsilon, I}| < 10^{1-\text{SNR}_a/10} * 0.5 \text{ dB}, \quad (14)$$

$$|\theta_{\epsilon, I}| < 10^{1-\text{SNR}_a/10} * 6^\circ. \quad (15)$$

The maximum bias errors were found by assuming  $A_s(f_p) \gg A_n(f_p)$ . Equations (17) and (18) are only valid, therefore, if the  $\text{SNR}_a$  is larger than about 10 dB. For  $\text{SNR}_a \geq 10$  dB, the magnitude error is always less than 0.5 dB and the angular error is always less than  $6^\circ$ . If instead the value of the  $\text{SNR}_a$  is 20 dB, the maximum angular error is less than  $1^\circ$ , while the magnitude error is imperceptible. Note also that these maximum errors decrease with a smaller separation angle between signal and broadband noise sources, which also serves to increase  $f_{\text{lim}}$ .

### C. Practical simplifications

For cases with a significantly large angular separation between the signal and additive noise sources,  $f_{\text{lim}}$  can actually be reached before the effective spatial Nyquist frequency for the probe,

$$f_{N, \text{eff}} = \min \left\{ \left| \frac{c}{2a \cos \theta_s} \right|, \left| \frac{c}{2a \sin \theta_s} \right| \right\}. \quad (16)$$

$$L_{\epsilon, I} = 10 \log_{10} \left( \frac{I_{\text{calc}}}{I} \right) \text{ dB}, \quad (10)$$

$$\theta_{\epsilon, I} = \theta_{\text{calc}} - \theta_s. \quad (11)$$

Using the PAGE method for acoustic vector intensity, the magnitude bias error in decibels at peak frequencies for the five-microphone probe in Fig. 2 is given by

When  $f_{\text{lim}} < f_{N, \text{eff}}$ , the additive noise negatively affects the PAGE method calculation of intensity below  $f_{N, \text{eff}}$ . In practice, to avoid negatively impacting calculation the angular separation should be limited to

$$|\theta_s - \theta_n| \leq 0.5 \text{ rad} \approx 28.6^\circ. \quad (17)$$

If Eq. (17) holds and  $4a\Delta f |\sin \theta_n| \ll c$ , then  $f_{\text{lim}}$  can be simplified as

$$f_{\text{lim}} \approx \frac{c}{4a|\theta_s - \theta_n|_{\text{rad}}}. \quad (18)$$

The maximum errors as a function of  $\text{SNR}_a$  then become

$$|L_{\epsilon, I}| < 10^{1-\text{SNR}_a/10} * 0.5 \text{ dB}, \quad (19)$$

$$|\theta_{\epsilon, I}| < 10^{1-\text{SNR}_a/10} * 2.5^\circ. \quad (20)$$

In summary, certain conditions must be met for the additive noise to be useful. First, the additive noise needs to be low-level relative to the signal, while still greater than the ambient noise level. Second, the angular separation between the signal and additive noise sources must not be too large. The frequency limit above which the additive noise is no longer particularly useful depends on this angular separation. Decreasing the angular separation increases the frequency

limit. The bias errors caused by the additive noise depend on the angular separation and the  $\text{SNR}_a$ , though a maximum error bound for frequencies below the frequency limit can be obtained by using the  $\text{SNR}_a$  value alone.

#### D. Guide to effective additive noise

Consolidating all of these approximations, guidelines emerge for when additive noise is useful and the accuracy of the resulting intensity calculation. For a plane-wave like signal, additive plane-wave noise is useful when

- signal and noise sources are separated by less than  $\sim 28^\circ$ , and
- $\text{SNR}_a \geq 10$  dB.

When these conditions are met,

- the upper frequency limit is  $f_{\text{lim}}$  as given in Eq. (18), and depends on the microphone spacing, sound speed, and angular separation of sources, and
- the calculated intensity magnitude and direction for frequencies below  $f_{\text{lim}}$  is always accurate to within 0.5 dB and  $2.5^\circ$ , respectively, of the analytical intensity. The accuracy increases with a decreasing angular separation and/or a larger  $\text{SNR}_a$ .

### III. ANALYTICAL RESULTS

Bias errors depend on how the data are processed. If  $\Delta f$  is negligibly small, and the  $\text{SNR}_a$  is large (greater than 20 dB), then the magnitude and direction intensity bias errors—shown in Figs. 3 and 4 as a function of  $ka$  and  $\theta_n$ , assuming  $\theta_s = 0^\circ$ —for a plane wave source can be obtained. The black line representing  $f_{\text{lim}}$  is shown: it outlines regions of high error, and delineates the frequency division above which additive noise is no longer helpful. There are two distinct overlapping error lobes seen—symmetric about  $\pm 90^\circ$  and  $\pm 180^\circ$ —

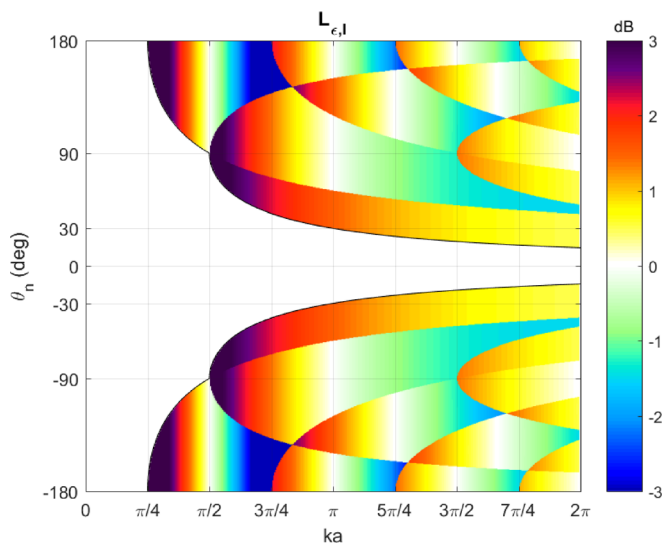


FIG. 3. (Color online) Analytical bias errors for PAGE-calculated intensity level for a plane wave source using the probe in Fig. 2, given as a function of  $ka$  and noise angle  $\theta_n$ , assuming  $\text{SNR}_a \geq 20$  dB and  $\theta_s = 0$ .

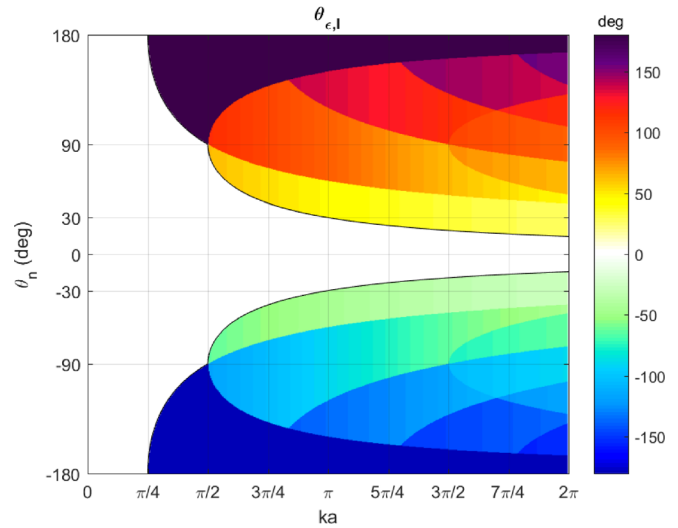


FIG. 4. (Color online) Analytical bias errors for PAGE-calculated intensity direction for a plane wave source using the probe in Fig. 2, given as a function of  $ka$  and noise angle  $\theta_n$ , assuming  $\text{SNR}_a \geq 20$  dB and  $\theta_s = 0$ .

whose lower bounds for  $ka$  coincide with the two different values for  $f_{\text{lim}}$  given in Eq. (8) (and multiples of these values), and give the limits for when the phase cannot be unwrapped in either one or both of the two orthogonal directions.

The analytical results are extremely promising: the errors below  $f_{\text{lim}}$  are small and are easily quantified. To allow for experimental verification, analytical results are shown for a specific example. The signal is a sawtooth source with low-level additive broadband brown noise. The sawtooth has a fundamental frequency of 250 Hz, with harmonic partials which decrease in amplitude. For frequencies that are not multiples of 250 Hz, the signal amplitude is very low, so  $A_s \approx 0$ . The low-level additive brown noise rolls off in a similar manner, such that the  $\text{SNR}_a$  at each peak frequency is approximately 34 dB, so  $A_s \gg A_n$  (this large  $\text{SNR}_a$  value is used because measurements were taken prior to analytically finding the limit of  $\text{SNR}_a \geq 10$  dB). Values of  $\theta_s = 0^\circ$ ,  $\Delta f = 1$  Hz,  $c = 343$  (m/s), and  $a = 5.08$  cm are used.

The analytical magnitude bias errors for this particular setup are shown in Fig. 5, while the analytical angular bias errors are shown in Fig. 6. The figures show the bias errors at the peak frequencies, plotted with an angular resolution of  $2.5^\circ$  with angular limits of  $\theta_n = \pm 90^\circ$ . The analytical bias errors below  $f_{\text{lim}}$  are the same as when no discrete processing resolution is assumed, but the error lobes seen above  $f_{\text{lim}}$  are fundamentally different because of the discrete frequency bin width—which results from using a finite sampling frequency and angular resolution rather than the continuous, analytical version shown previously.

Many horizontal lines appear in the bias error plots when using discrete values. They are caused by unwrapping errors, which, as previously noted, depend on the frequency bin width used in processing. At  $f_{\text{lim}}$ , or at the frequencies where one error lobe crosses another, the unwrapping errors propagate up to higher frequency bins. Despite the analytical differences when using a specific value  $\Delta f$ , there is no

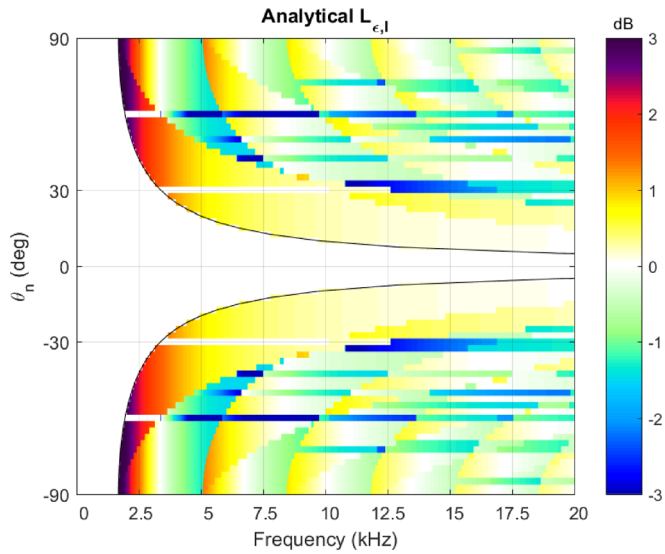


FIG. 5. (Color online) Analytical bias errors for PAGE-calculated intensity magnitude using the probe in Fig. 2 for a 250 Hz sawtooth source and additive noise with  $\theta_s = 0^\circ$ ,  $\Delta f = 1$  Hz,  $c = 343$  (m/s),  $a = 5.08$  cm, and  $\text{SNR}_a = 34$  dB. The black lines give the value of  $f_{\text{lim}}$ . A frequency of 3.376 kHz corresponds to  $ka = \pi$ .

discernable difference below  $f_{\text{lim}}$ , meaning bias errors in both magnitude and direction are still minimal.

#### IV. EXPERIMENTAL VERIFICATION

##### A. Experimental setup

The analytical bias errors in Figs. 5 and 6 are now compared to those obtained experimentally. Measurements were taken in the BYU fully anechoic chamber, which has a lower cutoff frequency of approximately 80 Hz. The microphone probe pictured in Fig. 2 was used, where the probe radius was  $a = 5.08$  cm. A loudspeaker generated a 250 Hz sawtooth wave signal and was placed on a stand such that  $\theta_s = 0^\circ$ . The

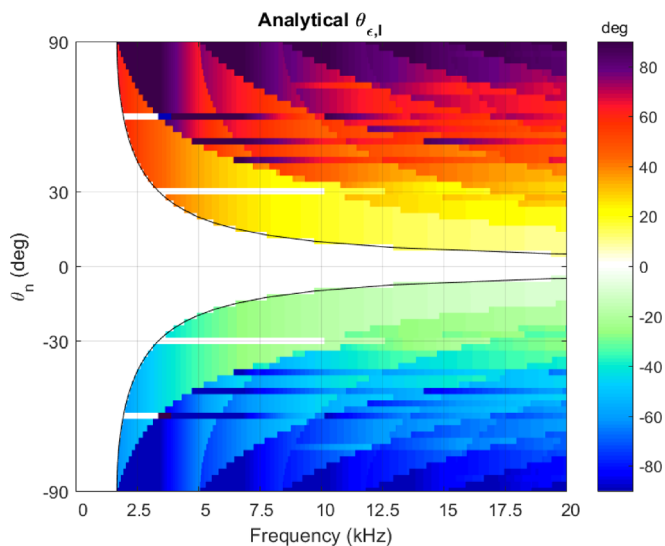


FIG. 6. (Color online) Analytical bias errors for PAGE-calculated intensity direction using the probe in Fig. 2 for a 250 Hz sawtooth source and additive noise with  $\theta_s = 0^\circ$ ,  $\Delta f = 1$  Hz,  $c = 343$  (m/s),  $a = 5.08$  cm, and  $\text{SNR}_a = 34$  dB. The black lines give the value of  $f_{\text{lim}}$ . A frequency of 3.376 kHz corresponds to  $ka = \pi$ .



FIG. 7. (Color online) Experimental setup. The source loudspeaker location is fixed, while the additive noise loudspeaker is on a rotating arm to have variable angular separation.

loudspeaker used for the additive noise was placed on the arm of a turntable which was rotated in angular increments of  $2.5^\circ$ . This second loudspeaker was raised slightly higher than the first, so that the speakers could be located the same distance—approximately 2 m—from the probe, but so that the rotating arm did not hit the first loudspeaker. The second loudspeaker on the arm broadcasted brown noise such that the  $\text{SNR}_a$  at peak frequencies was approximately 34 dB. Using this experimental setup, which is pictured in Fig. 7, and processing with a frequency bin width of  $\Delta f = 1$  Hz where the sound speed was  $c = 343$  (m/s), the results shown in Figs. 8 and 9 should ideally match the analytical results seen in Figs. 5 and 6, respectively.

##### B. Experimental results

Bias errors are found by comparing experimentally-obtained vector intensity to the analytical intensity for a 250 Hz sawtooth wave using Eqs. (10) and (11). The analytical angle for the intensity is  $0^\circ$ , so the direction bias errors, shown in Fig. 9, are simply

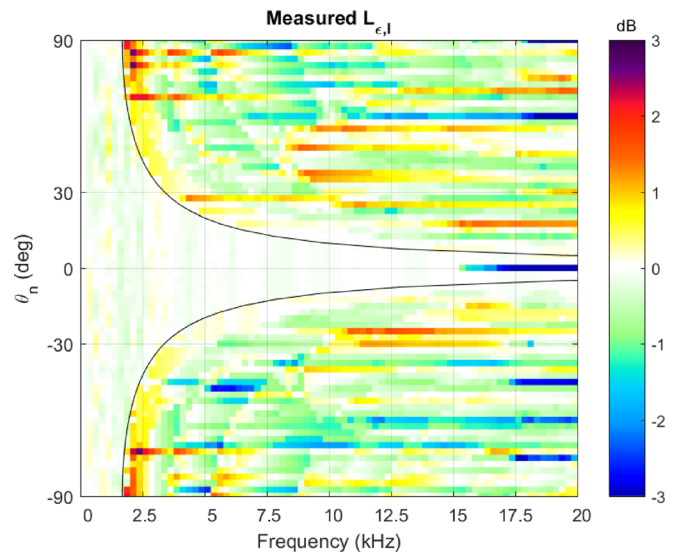


FIG. 8. (Color online) Experimental bias errors for PAGE-calculated intensity magnitude using the probe in Fig. 2 for a 250 Hz sawtooth signal and additive noise with  $\theta_s = 0^\circ$ ,  $\Delta f = 1$  Hz,  $c = 343$  (m/s),  $a = 5.08$  cm, and  $\text{SNR}_a = 34$  dB. The corresponding analytical level bias errors are seen in Fig. 5. A frequency of 3.376 kHz corresponds to  $ka = \pi$ .

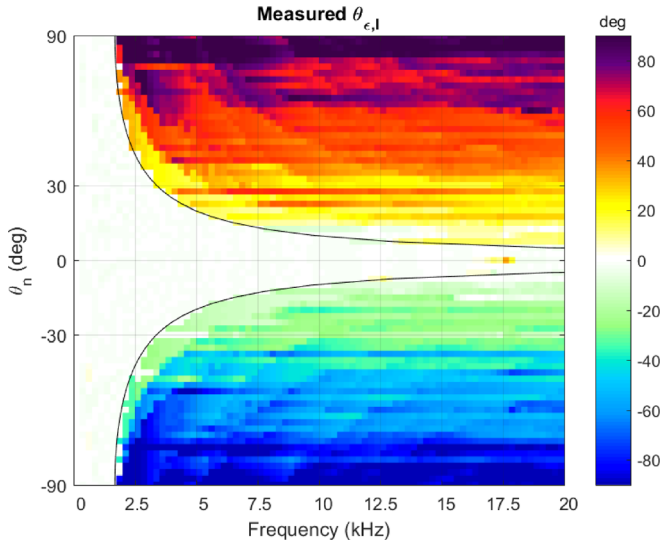


FIG. 9. (Color online) Experimental bias errors for PAGE-calculated intensity direction using the probe in Fig. 2 for a 250 Hz sawtooth signal and additive noise with  $\theta_s = 0^\circ$ ,  $\Delta f = 1$  Hz,  $c = 343$  (m/s),  $a = 5.08$  cm, and  $\text{SNR}_a = 34$  dB. The corresponding analytical direction bias errors are seen in Fig. 6. A frequency of 3.376 kHz corresponds to  $ka = \pi$ .

$$\theta_{\epsilon, I} = \theta_{\text{calc}}. \quad (21)$$

The analytical intensity magnitude is obtained by using the sound pressure level measured by the center microphone, and hence is  $G_{11}/\rho_0 c$ . The level bias errors, shown in Fig. 8, are then

$$L_{\epsilon, I} = 10 \log_{10} \left( \frac{L_{\text{calc}}}{G_{11}/\rho_0 c} \right). \quad (22)$$

The experimental results exhibit remarkable agreement with the analytical results. The frequency limit  $f_{\text{lim}}$  matches the analytical result. Above  $f_{\text{lim}}$ , the error lobe edges can be clearly seen, as can the horizontal lines caused by unwrapping with discrete frequency bins. Interestingly, the error lobes—though clearly present—are somewhat different than the analytical results. This is possibly caused by the inherent three-dimensional nature of the experimental setup.

Below  $f_{\text{lim}}$ , the errors are extremely small, with one noted exception; for  $\theta_n = 0^\circ$  the non-trivial error above around 15 kHz is caused by probe scattering.<sup>32</sup> The level bias is especially noticeable, because scattering off the front microphone shields the center microphone, the auto-spectrum of which is used to give the analytical intensity level. For this reason, other small, non-zero angular separation angles do not exhibit these increased bias errors. Below  $f_{\text{lim}}$ , the benefits of additive broadband noise are clearly manifest.

The benchmark spectral values, which are obtained from auto-spectral amplitudes, and the intensity levels calculated by the PAGE method are given in Fig. 10. The amplitude bias errors presented in this paper are calculated with benchmark and PAGE-calculated levels using Eqs. (12) and (13). The decreasing amplitude of sawtooth peaks, as well as the low-level additive noise, can be clearly seen in Fig. 10. The results presented clearly show that the additive noise has very little unintended effect on the calculated intensity, while the

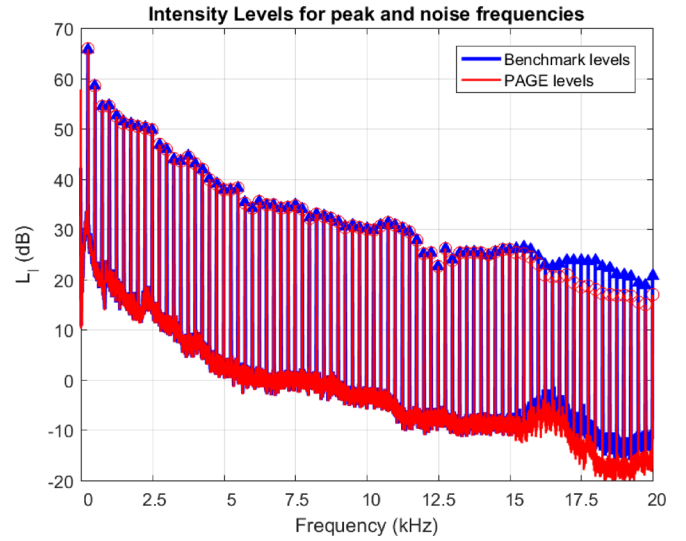


FIG. 10. (Color online) Spectral levels for the experimental setup using the probe in Fig. 2 for a 250 Hz sawtooth signal and additive noise with  $\theta_s = 0^\circ$ ,  $\theta_n = 0^\circ$ ,  $\Delta f = 1$  Hz,  $c = 343$  (m/s),  $a = 5.08$  cm, and  $\text{SNR}_a = 34$  dB. The bias errors are given by the difference between the benchmark values (obtained from auto-spectral amplitudes) and the calculated PAGE levels. The peak frequencies shown correspond to the frequencies plotted in previous figures.

additional phase information vastly improves intensity calculation above the spatial Nyquist frequency.

## V. CONCLUSIONS

When certain conditions are met, adding broadband noise to narrowband signals can greatly improve the calculation of active acoustic intensity using the PAGE method. Below the spatial Nyquist frequency, the PAGE method can obtain accurate intensity vectors with or without additive noise. Above the spatial Nyquist frequency, the additive broadband noise provides phase information to improve unwrapping, which yields more accurate intensity vectors. The conditions for when additive noise is beneficial are (1) when the signal-to-additive-noise ratio,  $\text{SNR}_a$ , should exceed 10 dB at peak frequencies, and (2) when the signal and additive noise sources should be separated by less than  $\sim 28^\circ$ . An upper frequency limit  $f_{\text{lim}}$  can be computed from the angular separation, sound speed, and microphone spacing, using Eq. (18), above which additive noise is no longer beneficial. These conclusions are supported by both analytical and experimental verification.

For certain probe configurations, scattering can occur before  $f_{\text{lim}}$  is reached. To reduce scattering, a greater microphone separation distance is beneficial.<sup>32</sup> Probe rotation such that microphones no longer shield one another is also a viable option. Increasing the microphone separation also decreases the spatial Nyquist frequency, which reduces the usable bandwidth when using the traditional method for calculating intensity; for the PAGE method, a greater microphone separation distance decreases  $f_{\text{lim}}$ , though as the angular separation between the signal and additive noise source goes to zero,  $f_{\text{lim}}$  becomes infinite. The experimental upper frequency limit necessarily depends on probe

scattering, microphone spacing, and angular separation of the sources.

As a general guideline, a smaller angular separation between the signal and the additive broadband noise source can yield a higher upper frequency limit for PAGE-based intensity calculation of narrowband noise. As long as the SNR<sub>a</sub> exceeds 10 dB at peak frequencies, the intensity bias errors are minimal—within 0.5 dB and 2.5° of the magnitude and direction of the analytical intensity. These errors decrease with increasing SNR<sub>a</sub> and decreasing angular separation. The addition of additive low-level broadband noise to band-limited signals serves to improve PAGE-calculated intensity values.

<sup>1</sup>J. A. Mann and J. Tichy, “Near-field identification of vibration sources, resonant cavities, and diffraction using acoustic intensity measurements,” *J. Acoust. Soc. Am.* **90**, 720–729 (1991).  
<sup>2</sup>F. Jacobsen, “Spatial sampling errors in sound power estimation based upon intensity,” *J. Sound Vib.* **145**, 129–149 (1991).  
<sup>3</sup>F. J. Fahy, *Sound Intensity* (Thomson Press, Bury St Edmunds, Suffolk, UK, 1995).  
<sup>4</sup>ANSI/ASA S1.9:1996: *Instruments for the Measurement of Sound Intensity* (Acoustical Society of America, Melville, NY, 1996).  
<sup>5</sup>F. J. Fahy, “Measurement of acoustic intensity using the cross-spectral density of two microphone signals,” *J. Acoust. Soc. Am.* **62**, 1057–1059 (1977).  
<sup>6</sup>G. Pavić, “Measurement of sound intensity,” *J. Sound Vib.* **51**, 533–545 (1977).  
<sup>7</sup>J. Y. Chung, “Cross-spectral method of measuring acoustic intensity without error caused by instrument phase mismatch,” *J. Acoust. Soc. Am.* **64**, 1613–1616 (1978).  
<sup>8</sup>F. Jacobsen, “Intensity techniques,” in *Handbook of Signal Processing in Acoustics* (Springer, New York, 2008), pp. 1109–1127.  
<sup>9</sup>F. Jacobsen, “Sound intensity,” in *Springer Handbook of Acoustics* (Springer, New York, 2007), pp. 1053–1075.  
<sup>10</sup>F. Jacobsen, “Random errors in sound intensity estimation,” *J. Sound Vib.* **128**, 247–257 (1989).  
<sup>11</sup>A. F. Seybert, “Statistical errors in acoustic intensity measurements,” *J. Sound Vib.* **75**, 519–526 (1981).  
<sup>12</sup>T. Loyau and J.-C. Pascal, “Statistical errors in the estimation of the magnitude and direction of the complex acoustic intensity vector,” *J. Acoust. Soc. Am.* **97**, 2942–2962 (1995).  
<sup>13</sup>C. P. Wiederhold, K. L. Gee, J. D. Blotter, and S. D. Sommerfeldt, “Comparison of methods for processing acoustic intensity from orthogonal multimicrophone probes,” *J. Acoust. Soc. Am.* **131**, 2841–2852 (2012).  
<sup>14</sup>J.-C. Pascal and J.-F. Li, “A systematic method to obtain 3D finite-difference formulations for acoustic intensity and other energy quantities,” *J. Sound Vib.* **310**, 1093–1111 (2008).  
<sup>15</sup>C. P. Wiederhold, K. L. Gee, J. D. Blotter, S. D. Sommerfeldt, and J. H. Giraud, “Comparison of multimicrophone probe design and processing methods in measuring acoustic intensity,” *J. Acoust. Soc. Am.* **135**, 2797–2807 (2014).

<sup>16</sup>F. Jacobsen, “A simple and effective correction for phase mis-match in intensity probes,” *Appl. Acoust.* **33**, 165–180 (1991).  
<sup>17</sup>T. Yanagisawa and N. Koike, “Cancellation of both phase mismatch and position errors with rotating microphones in sound intensity measurements,” *J. Sound Vib.* **113**, 117–126 (1987).  
<sup>18</sup>T. Iino, H. Tatekawa, H. Mizukawa, and H. Suzuki, “Numerical evaluation of three-dimensional sound intensity measurement accuracies and a proposal for an error correction method,” *Acoust. Sci. Technol.* **34**, 34–41 (2013).  
<sup>19</sup>D. K. Torrie, E. B. Whiting, K. L. Gee, T. B. Neilsen, and S. D. Sommerfeldt, “Initial laboratory experiments to validate a phase and amplitude gradient estimator method for the calculation of acoustic intensity,” *Proc. Mtgs. Acoust.* **23**, 030005 (2015).  
<sup>20</sup>D. C. Thomas, B. Y. Christensen, and K. L. Gee, “Phase and amplitude gradient method for the estimation of acoustic vector quantities,” *J. Acoust. Soc. Am.* **137**, 3366–3376 (2015).  
<sup>21</sup>B. Y. Christensen, “Investigation of a new method of estimating acoustic intensity and its application to rocket noise,” Master’s thesis, Brigham Young University, Provo, UT, 2014.  
<sup>22</sup>J. A. Mann, J. Tichy, and A. J. Romano, “Instantaneous and time-averaged energy transfer in acoustic fields,” *J. Acoust. Soc. Am.* **82**, 17–30 (1987).  
<sup>23</sup>J. A. Mann and J. Tichy, “Acoustic intensity analysis: Distinguishing energy propagation and wave-front propagation,” *J. Acoust. Soc. Am.* **90**, 20–25 (1991).  
<sup>24</sup>K. F. Succo, S. D. Sommerfeldt, K. L. Gee, and T. B. Neilsen, “Acoustic intensity of narrowband sources using the phase and amplitude gradient estimator method,” *Proc. Mtgs. Acoust.* **30**, 030015 (2017).  
<sup>25</sup>D. C. Ghiglia and M. D. Pritt, *Two-Dimensional Phase Unwrapping: Theory, Algorithms, and Software* (Wiley New York, 1998).  
<sup>26</sup>T. A. Stout, K. L. Gee, T. B. Neilsen, A. T. Wall, and M. M. James, “Source characterization of full-scale jet noise using acoustic intensity,” *Noise Control Eng. J.* **63**, 522–536 (2015).  
<sup>27</sup>K. L. Gee, T. B. Neilsen, S. D. Sommerfeldt, M. Akamine, and K. Okamoto, “Experimental validation of acoustic intensity bandwidth extension by phase unwrapping,” *J. Acoust. Soc. Am.* **141**, EL357–EL362 (2017).  
<sup>28</sup>K. L. Gee, T. B. Neilsen, E. B. Whiting, D. K. Torrie, M. Akamine, K. Okamoto, S. Teramoto, and S. Tsutsumi, “Application of a phase and amplitude gradient estimator to intensity-based laboratory-scale jet noise source characterization,” in *Proceedings of the Berlin Beamforming Conference*, Berlin, Germany (February 24–25, 2016), Paper No. BeBeC-2016-D3.  
<sup>29</sup>K. L. Gee, M. Akamine, K. Okamoto, T. B. Neilsen, M. R. Cook, S. Teramoto, and T. Okunuki, “Characterization of supersonic laboratory-scale jet noise with vector acoustic intensity,” in *Proceedings of the 23rd AIAA/CEAS Aeroacoustics Conference*, Denver, CO (June 5–9, 2017), p. 3519.  
<sup>30</sup>M. R. Cook, K. L. Gee, T. B. Neilsen, and S. D. Sommerfeldt, “The effects of contaminating noise on the calculation of acoustic intensity for pressure gradient methods,” *J. Acoust. Soc. Am.* **145**, 173–184 (2019).  
<sup>31</sup>M. R. Cook, K. L. Gee, S. D. Sommerfeldt, and T. B. Neilsen, “Coherence-based phase unwrapping for broadband acoustic signals,” *Proc. Mtgs. Acoust.* **30**, 055005 (2017).  
<sup>32</sup>M. T. Rose, R. D. Rasband, K. L. Gee, and S. D. Sommerfeldt, “Comparison of multi-microphone probes and estimation methods for pressure-based acoustic intensity,” *Proc. Mtgs. Acoust.* **26**, 030004 (2016).